EXPERIMENTAL INVESTIGATION OF AUTOMOTIVE COMPONENTS CONSISTING OF HYBRID FRP-METAL-MATERIAL SYSTEMS UNDER DYNAMIC LOADING

Michael Dlugosch[1], Dirk Lukaszewicz[2], Jens Fritsch[1] and Stefan Hiermaier[1]

[1]Fraunhofer Institute for Highspeed Dynamics, Ernst-Mach-Institute, EMI, Department of Material Dynamics, Eckerstrasse 4, 79104 Freiburg, Germany
Email: Michael.dlugosch@emi.fraunhofer.de, Web Page: http://www.emi.fraunhofer.de/
[2]Department of Passive Safety, BMW Group, Knorrstrasse 147, 80788 Munich, Germany

Keywords: Automotive, hybrid material systems, dynamic testing, crash loading, experimental

Abstract
Generic components comprised of hybrid material systems consisting of steel and advanced composites are dynamically tested under axial impact and bending. A hybridization of composite base structures significantly affects the specimens' behavior and the failure pattern. Particularly when considering such aspects as compatibility and scaleability these hybrid structures could outperform conventional and pure composite solutions.

1. Introduction

Motivated by efficiency goals and upcoming strict *EU*-regulations for CO_2 emissions [1], lightweight design plays an increasingly important role in automotive engineering. Since the load carrying structures in the body-in-white (*BiW*) comprise ca. 25 % of the entire vehicle weight it is a very promising system for the application of effective lightweight design measures [2].
Novel materials are one way to reduce the weight of the body-in-white while simultaneously meeting the growingly stringent crash safety requirements. Advanced composites like carbon or glass fiber reinforced plastics (*CFRP*/*GFRP*) exhibit weight specific crashworthiness characteristics that, though strongly dependent on the composite's constituents and their arrangement, mostly outrival those of metals [3–5]. Metals in turn offer relatively cost efficient solutions with well understood and stable energy absorbing mechanisms. This study explores the possibilities to form synergetic "hybrid" combinations of those different types of materials aiming to exploit their respective benefits in future crash structural applications.
Research on the mechanical behavior of hybrid material systems consisting of advanced composites and metals so far mostly originated from direct applications in complex engineering systems rather than in the field of fundamental material research. In the 1990s Ford produced a high volume vehicle with a hybrid front end structure composed of a sheet steel framework and injection molded rib reinforcements of glass fiber reinforced polyamide [6]. Next to weight specific increases in strength and stiffness they discovered high integrative potential and good recyclability. Further investigations on hybrid structural automotive components like b-pillars, door sills and roof or floor structures have been conducted by several authors [7–11]. These investigations were often embedded in industry-oriented research projects that resulted in case and feasibility studies concerning direct applications of hybrid structures with respect to weight savings, production techniques and costs. As a general result, those hybrid structures could be identified as feasible solutions in the respective fields of application with the possibility of moderate to high weight savings, higher integration levels and/or enhanced mechanical properties compared to conventional solutions.
Focusing on the mechanics and the crashworthiness of hybrid structures in automotive crash applications Wang et al. [12] conducted quasi static and dynamic impact tests on steel cylinders circumferentially wrapped with *GFRP* and found the composite material to be an effective

Excerpt from ISBN 978-3-00-053387-7

reinforcement to the tubes. According to their results the strengthening effect grew with an increasing composite to steel ratio, eventually leading to an altered, more effective failure mode. Disadvantageous changes in the damageing mode were observed by *Bouchet* et al. [13] while crushing aluminum cylinders circumferentially wrapped with *GFRP*. A dependency on the thickness of the tube as well as on the composite reinforcement was found, but no correlation to any sort of surface treatment at the bonding interface. Similar findings were made by *Shin* et al. [14] wrapping *GFRP* prepregs around square aluminum tubes. In quasi static crushing tests they discovered a specific reinforcing effect of *GFRP* depending on the ply orientations and the composite thickness. Kim at al. [15] also studied the crashworthiness of aluminum square tubes reinforced with CFRP subjected to axial low velocity impact. They found that *CFRP* reinforcements enhanced both the CFE (crush force efficiency) and the *SEA* (weight specific crash energy absorption capability) of the crush tubes by 30 % and 38 % respectively. Related studies were conducted by *Bambach* et al. [16–22]. The authors analyzed the reinforcing effect of externally applied *CFRP* on crush tubes of different specifications. The influences of the tube design and material as well as the number and orientation of the *CFRP* layers on the crash characteristics were investigated. They found substantial improvements in crash performance compared to tubes made of one single material (*Mamalis* [23]). However, the impact characteristics of composite crush tubes strongly depend on the complex failure mechanisms within the material [24] and thus have a vast range of values for their metrics of crashworthiness such as the *LU* ("load uniformity") or *SEA* ("specific energy absorption"). Considering other factors such as geometric, bonding or architectural aspects, a direct comparison between the different material systems is difficult. The abovementioned scientific publications indicate significant weight saving potentials inherent in hybrid materials comprised of fiber reinforced plastics and metals. They also indicate their strong dependency on their architectural design and single material constituents. Thus, the conclusions drawn from the test results can only be valid for the respective set of parameters (e.g. specimen geometry) and can hardly be transferred to other settings or even be generalized.

Based on a large experimental study on the characterization of these hybrid material systems on a coupon scale previously conducted by the authors [25], the present study focuses on the dynamic loading of automotive components composed of hybrid material systems under axial compression. The hybrid components studied here follow the concept of composite-intensive hybrids rather than conventional metallic structures reinforced with advanced composites. The aim is to confirm and complement the findings of the previous studies in terms of the effects of major design parameters and the identification of hybrid mechanisms as well as the full exploitation of the composites' potentials in crash structural applications.

2. Specimens details and experimental procedures

2.1. Constituent materials

In order to represent a type of steel commonly used in the BiW a dual phase steel named "HCT600X+Z100" [26] – genrally applied in energy absorbing structures – is used for the manufacturing of the reinforcement shells. The name is abbreviated as "*DPS*" (Dual Phase Steel) below. The composite layups were manufactured using unidirectional glass or carbon fiber mats pre-impregnated with epoxy resin (prepregs). Both the carbon fiber prepreg "PREDO PR-UD CS 300/600 FT 102 38" [27] and the glass fiber prepreg "PREDO PR-UD EST 300/300 FT 102 35" [28] were produced by SGL epo GmbH. To ensure comparability both prepregs contained the same epoxy resin matrix "FT102" [29] and had a fiber areal weight of 300 g/m^2. The fiber mass fractions were 62 % and 65 % for the carbon and the glass fiber prepreg, respectively. The types of reinforcing fibers used in this study were 50k filaments industrial grade carbon fibers and standard E-glass fibers, which are commonly used in engineering applications such as automotive or aircraft systems.
Joining of the constituents was achieved through a layer of "BETAMATE 2096" [30], a two-component epoxy structural adhesive widely used in the automotive sector for structural applications and repair. This type of adhesive has proven to be suitable for joining composites and metals in previous test series [31].

Excerpt from ISBN 978-3-00-053387-7

2.1. Specimen design, variants and manufacturing

As schemtically depicted in Figure 1 the specimens consisted of a 16-plied *FRP* base structure externally reinforced with adhesively bonded steel shells. The length of the specimens was 800 mm and 400 mm for the bending and the axial compression specimens, respectively.

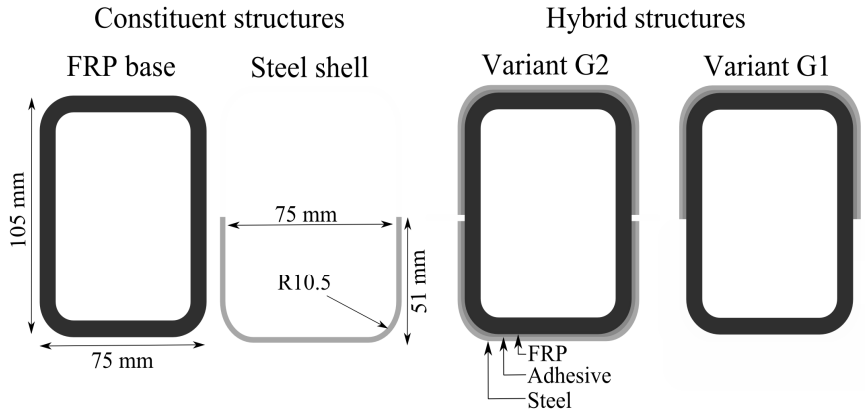

Figure 1. Cross-sectional view of the designs of the hybrid specimens composed of a *FRP* base structure and adhesively bonded reinforcing steel shells.

While the thickness of the adhesive layer was 0.2 mm, the ply thicknesses for *CFRP* and *GFRP* were 0.36 and 0.26 respectively yielding different steel-to-*FRP* ratios for the respective fibers. Table 1 shows the entire list of tested variants comprising two designs (*G1* and *G2*), two types of fibers and steel thicknesses and two types of 16-plied symmetric layups. The layup selection is based on the findings made by the authors in previous studies (see [25]).

Table 1. Specimen codes and parameter settings of all variants tested.

Specimen Code	Reinforcement Design	Steel thickness [mm]	Type of Fiber	Fiber Layup
G1-1.5-C-90	*G1*	1.5	Carbon	$[0/90]_{S,4}$
G2-1.5-C-90	*G2*	1.5	Carbon	$[0/90]_{S,4}$
G1-1.0-C-45	*G1*	1.0	Carbon	$[-45/0/45/0]_{2S}$
G2-1.0-C-45	*G2*	1.0	Carbon	$[-45/0/45/0]_{2S}$
G1-1.0-C-90	*G1*	1.0	Carbon	$[0/90]_{S,4}$
G2-1.0-C-90	*G2*	1.0	Carbon	$[0/90]_{S,4}$
G1-1.5-G-45	*G1*	1.5	E-Glass	$[-45/0/45/0]_{2S}$
G2-1.5-G-45	*G2*	1.5	E-Glass	$[-45/0/45/0]_{2S}$
G1-1.5-G-90	*G1*	1.5	E-Glass	$[0/90]_{S,4}$
G2-1.5-G-90	*G2*	1.5	E-Glass	$[0/90]_{S,4}$
G1-1.0-G-45	*G1*	1.0	E-Glass	$[-45/0/45/0]_{2S}$
G2-1.0-G-45	*G2*	1.0	E-Glass	$[-45/0/45/0]_{2S}$
C-90	-	-	Carbon	$[0/90]_{S,4}$
G-90	-	-	E-Glass	$[0/90]_{S,4}$

In the manufacturing process the prepregs were manually layered according to the stack of fiber angles in the respective layup and then cured in the autoclave. The closing of the section was achieved through shafting the prepregs using a specifically designed tool (Figure 2).

Excerpt from ISBN 978-3-00-053387-7

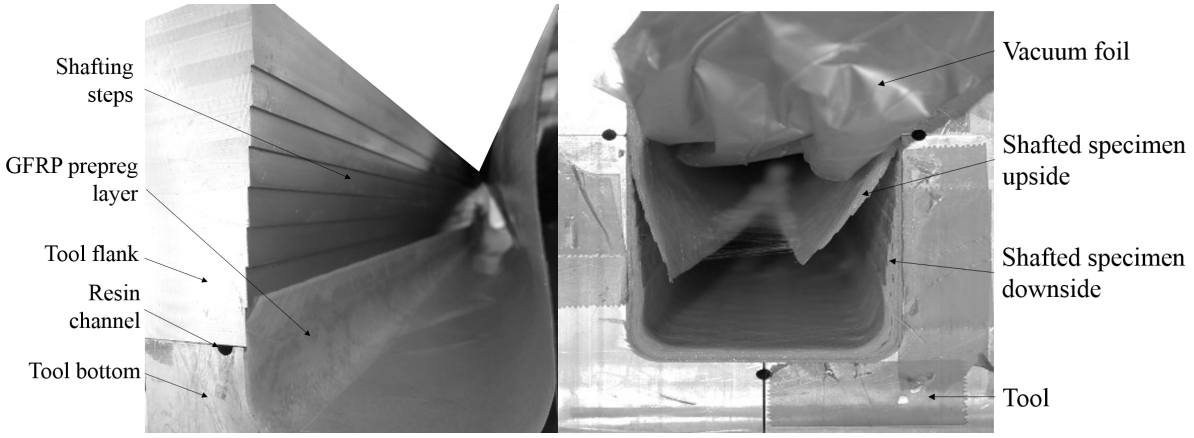

Figure 2. Open manufacturing tool with shafting steps (left) and closed tool for the *FRP* closed-section base structures.

The bent steel shells were bonded to the cured *FRP* base structure after roughening and cleaning of its surfaces. Finally, the axial compression specimens were bonded to a mounting plate and a 15° arrow trigger was cut to the specimens' top to ensure a stable onset of the progressive damage (see Figure 6).

2.1. Testing procedures and evaluation metrics

All axially loaded specimens were tested in the component crash test facility at the Fraunhofer EMI crash center schematically pictured in Figure 3 (left). The dynamic expansion of the air inside a pressure vessel with up to 200 bar propels a push rod and a guided sled of variable mass which then impacts the specimen mounted at the abutment. The testing speed was 8.3 m/s (±0.1) while the kinetic energy was varied according to the anticipated mean crush force of the variant by adjusting the mass of the sled (315 – 795 kg). The force was recorded by a sensor mounted between the bottom plate of the specimen and the abutment. All bending specimens were tested in a drop tower (depicted on the right side of Figure 3) at the EMI material laboratory using two 3D force sensors.

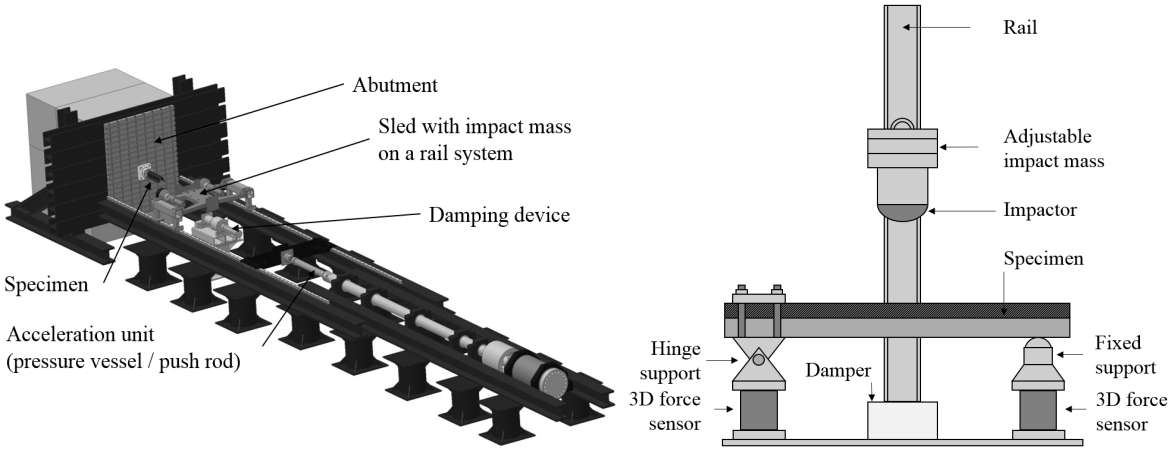

Figure 3. Component crash test facitlity at the Fraunhofer EMI crash center (left) and the drop tower testing rig for the bending specimens (right).

The bending test setup was derived from a b-pillar loading situation in a side barrier test, such as the IIHS-test. Here, the b-pillar-roof connection works as a hinge and the fender connection provides the possibility of material flow towards the location of impact. The impactor's velocity and mass were

Excerpt from ISBN 978-3-00-053387-7

varied (5.9 – 9.6 m/s and 27 – 80 kg, respectively) in order to cause large specimen deformations without catastrophic failure.
The displacement and speed of the sleds were measured using a magnetic transient recorder. High speed (*HS*) video recordings were made in order to qualitatively assess the damaging process and to provide for possibilities of optical measurements of spatial displacement. Each variant was tested twice to check for the reproducibility of the crushing behavior. All force signals were processed using filters (butterworth low-pass of orders 4 - 5) to reduce vibrations in the signal.
Next to the qualitative assessment of the different variants' behavior by interpreting load-displacement plots and analyzing failure patterns, several performance metrics have been evaluated. Figure 4 (left) depicts the typical force-displacement plot of an axially loaded hybrid specimen including some crucial parameter definitions.

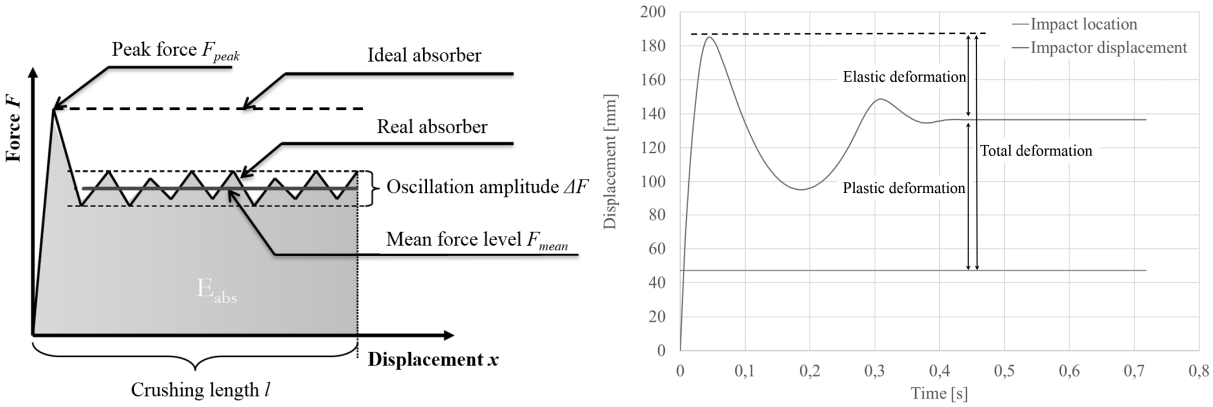

Figure 4. Schematic force-displacement plot of an axially loaded specimen (left, reprod. from [32]) and a displacement-time plot of the impactor during a drop tower bending test (right).

Considering the application background of this study, the (mass-) specific energy absorption *SEA* is the most important performance metric. It is defined as

$$SEA = \frac{1}{m(l)} \cdot \int_{l} F(x), \tag{1}$$

where *m(l)* is the mass of the crushed specimen length *l* and $\int_{l} F(x)$ equals the energy absorbed by the specimen, which can be interpreted as the area underneath the force-displacement graph (gray area in Figure 4). Further metrics to assess the quality of an absorbing structure are the load uniformities LU_I and LU_{II}, which are defined as

$$LU_I = \frac{F_{peak}}{F_{mean}} \text{ and } LU_{II} = \frac{\Delta F}{F_{mean}}. \tag{2}$$

Here, F_{peak} is the maximum force usually observed at the onset of the progressive damage and generally highly dependent on the type of trigger [24]. F_{mean} is the arithmetic mean of the force signal excluding the initial peak force and ΔF is the oscillation amplitude. In the design of automotive crash structures an ideal absorber would yield a LU_I-value of 1 and a LU_{II}-value of 0.
The right graph in Figure 4 depicts a plot of the impactor displacement over time in a bending test. The location of impact-line depicts the first contact of the impactor with the specimen. The dashed line indicates the maximum displacement followed by a varying number of rebounds. Considerung the final deflection of the impactor as well, the total deformation and its plastic share R_{plast} can be determined by solving the equation

Excerpt from ISBN 978-3-00-053387-7

$$R_{plast} = \frac{D_{plast}}{D_{total}} . \quad (3)$$

A deformation – or intrusion – relative to the impact energy D_{rel} is described as

$$D_{rel,spec} = \frac{D_{total} \cdot m_{specimen}}{E_{impact}} , \quad (4)$$

Where E_{impact} is the impact energy comprising a kinetic and a potential share and $m_{specimen}$ is the specimen's mass. Additionally the maximum force can be evaluated as a quantitative metric.

3. Results and discussion

The results section in this paper will be devided into two parts – the axial impact tests and the bending tests, both of which comprise qualitative aspects, such as the failure pattern and the shape of the load-displacement plot and a quantitative part, which focuses on the performance metrics defined above. Generally, only a subset of results can be presented due to reasons of scope of this paper.

3.1. Axial impact tests

Qualitative - Figure 5 depicts a force-displacement plot of an axially impacted hybrid specimen on the left and a selection of frames of the indicated time steps on the right side.

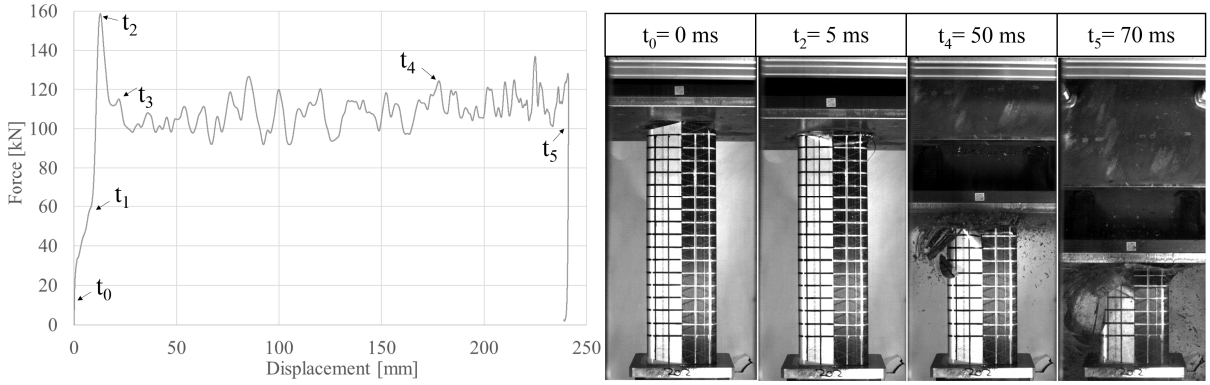

Figure 5. Force-displacement plot of an axially crushed hybrid specimen (left) and corresponding *HS*-video frames (right).

At t_0 the impactor sled reaches the tip of the specimen trigger, which is then fully crushed at t_1. As the plate impacts the entire cross sectional area of the specimen the force increases to its peak value at t_2. The mean force is evaluated between the starting point of the stable progressive crushing at t_3, passing t_4 to the rebound of the impactor at t_5.
As to be seen in Figure 6 the hybridization has a significant effect on the failure mechanism of the *FRP*. In combination with *CFRP* the steel reinforcement induces a higher level of disintegration and promotes the creation of new surfaces, which especially observed for $[-45/0/45/0]_{2S}$-laminates. *GFRP* in turn is urged to fold into the inside cavity of the specimen.

Excerpt from ISBN 978-3-00-053387-7

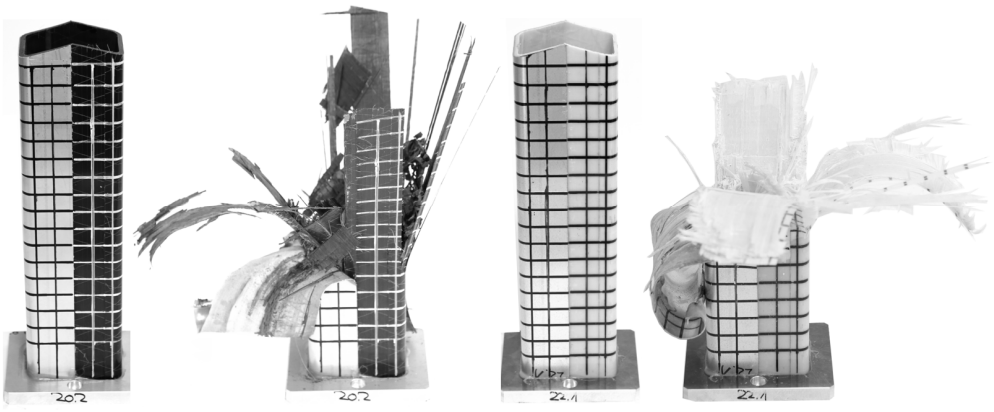

Figure 6. *G1-CFRP* (left) and *G1-GFRP* (right) specimens before and after axial impact testing.

The laminates generally exhibit extensive delaminations into single plies. The steel shell shows two different major failure patterns – an outside fold with shear wrinkles and an edge-ripping with rolling of the sides. While there is no significant correlation to the parameters of variation, the continuous rolling of the steel shell seems to promote a lower level of oscillation and thus more constant behavior of the crushing force. Generally, the repeatability proved to be very good in terms of the force-displacement measurements.

Quantitative - Figure 7 displays the *SEA*-values for the different hybrid and pure *FRP*-variants tested.

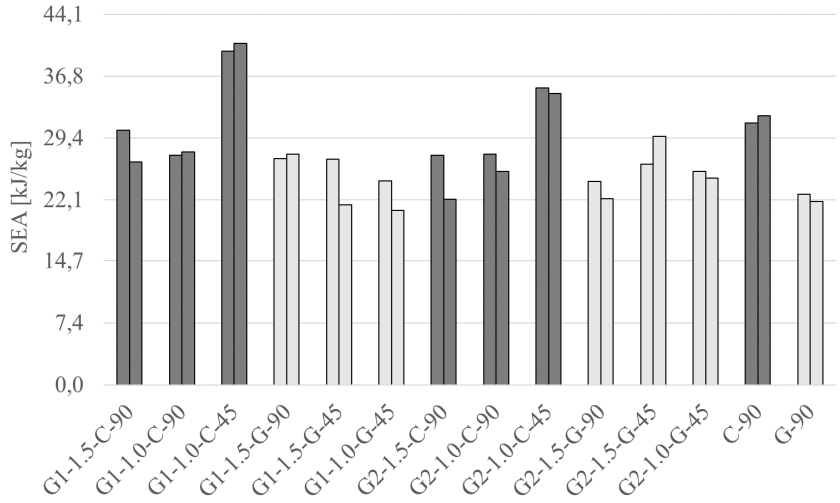

Figure 7. Specific energy absorption (*SEA*) of the hybrid and pure FRP variants under axial impact.

It is observed that only *GFRP*-hybrids yield a higher *SEA* than the respective pure *FRP* specimen, where *CFRP* exhibits a 29 % higher value than *GFRP*. While there is no significant dependency for *GFRP*-hybrids, the G1-reinforcement yields a higher *SEA* for *CFRP*-variants. The steel thickness does not affect the *SEA* significantly. The $[-45/0/45/0]_{2S}$-layup however outperforms the $[0/90_2/0]_{2S}$-layup, which is particularly seen for *CFRP*. This correlates with a higher level of disintegration described above.

Figure **8** depicts the load uniformities LU_I and LU_{II} as derived above. In contrast to *GFRP*, pure *CFRP* yields a lower (better) LU_I than its respective hybrid variant. Generally, *G2*-reinforcements yield a better LU_I than *G1*, which indicates advantageous properties of fully hybridized variants.

Excerpt from ISBN 978-3-00-053387-7

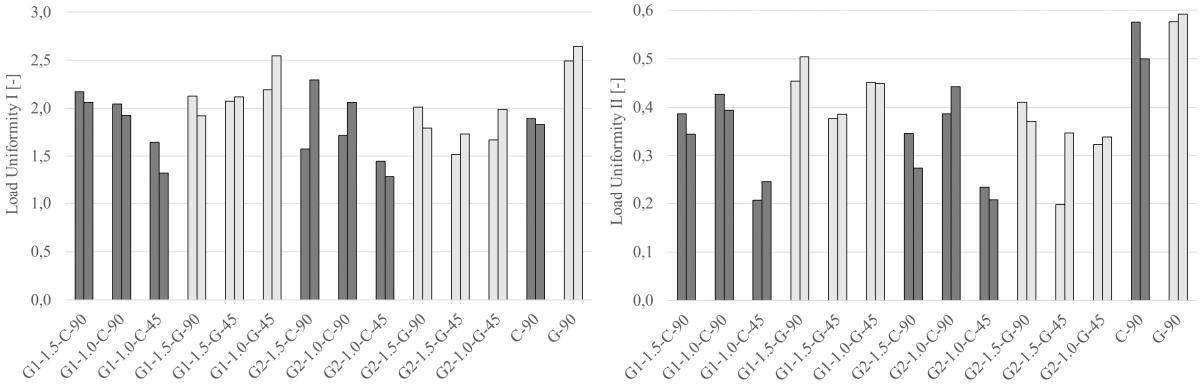

Figure 8. Load uniformity I (LU_I, left) and II (LU_{II}, right) for all hybrid and pure *FRP* specimens.

While there is no correlation for *CFRP*, thicker steel yields slightly better LU_I-values for *GFRP* variants. However, the layup tends to only affect the LU_I of *CFRP* hybrids, where again the C-1.0-45 variants show the best performance. It is noted, that the LU_I is also highly dependent of the trigger type at the specimens' tip. Regarding the LU_{II}, the $[-45/0/45/0]_{2S}$-layup yields smaller (e.g. better) values than the $[0/90]_{S,4}$-layup, which is particularly observed for *CFRP*, which generally exhibits lower values than *GFRP*. The type of reinforcement has no effect on the LU_{II} of *CFRP* but improves the values of *GFRP* variants.

3.1. Bending tests

Qualitative - Figure 9 depicts a typical force-displacement plot of a dynamic bending test and the corresponding HS-video frames as indicated.

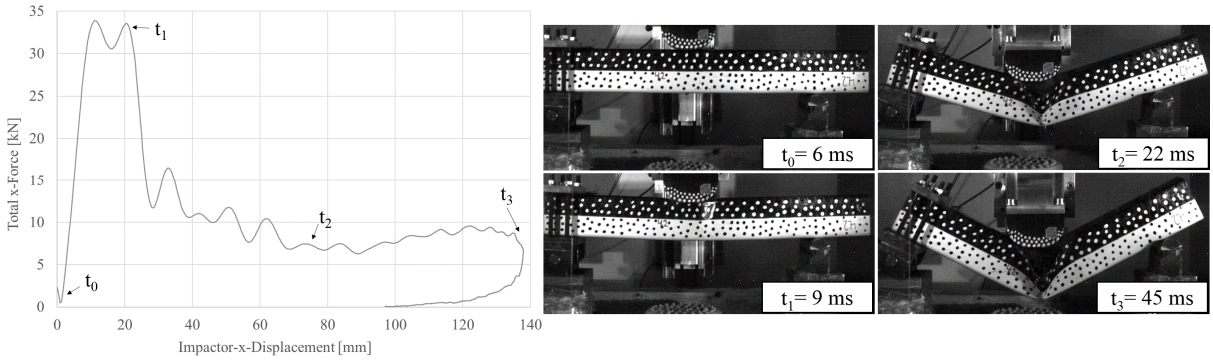

Figure 9. Force-displacement plot of a drop tower bending test (left) and the corresponding HS-video frames (right).

After the impact at t_0, the force rises to a maximum until a first specimen buckling is detected in the video at t_1. Passing t_2, the specimen resists the deformation with an individual force level / profile until the first rebound of the impactor at t_3. Figure 10 depicts impacted bending specimens with corresponding parameter settings and the same amount of impact energy for the *G1*- and the *G2*-variants, respectively.

Excerpt from ISBN 978-3-00-053387-7

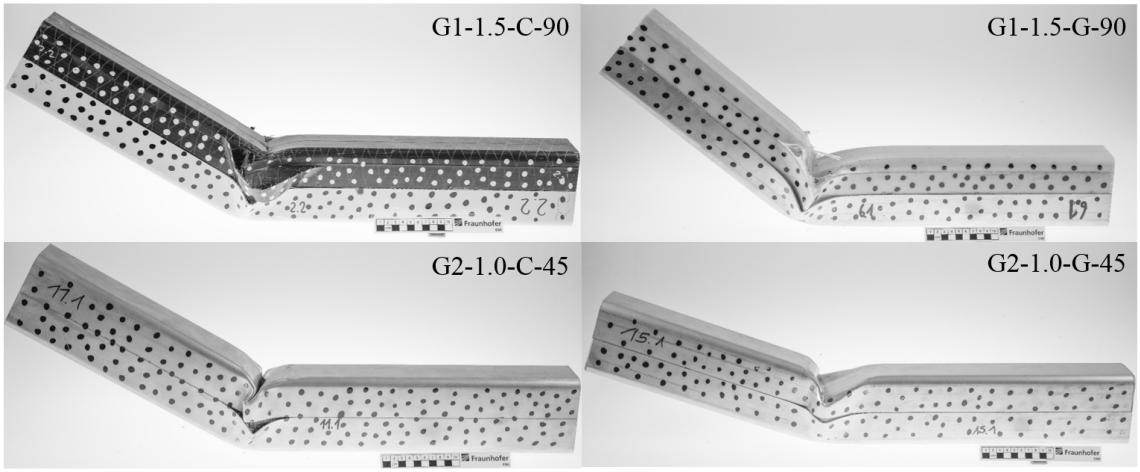

Figure 10. Corresponding pairs of *G1*- and *G2*-specimens, respectively impacted with the same amount of energy.

It is observed that for the *G1*-specimens the total plastic deformation of *GFRP* is higher than for *CFRP* - as opposed to the *G2*-specimens exhibiting a contrary effect of the fiber type. Generally, the size of the damaged area and the severity of the failure mechanisms observed is greater for *CFRP*- than for *GFRP*-hybrids. While the first pure *CFRP*-specimen fails catastrophically (complete separation of the specimens' halves) the pure *GFRP*-variant barely shows any outer signs of damage after bearing the same impact energy.

Quantitative - Figure 11 depicts the energy- and mass-specific deformation $D_{rel,spec}$ (left) and the ratio of plastic to total deformation R_{plast} (right).

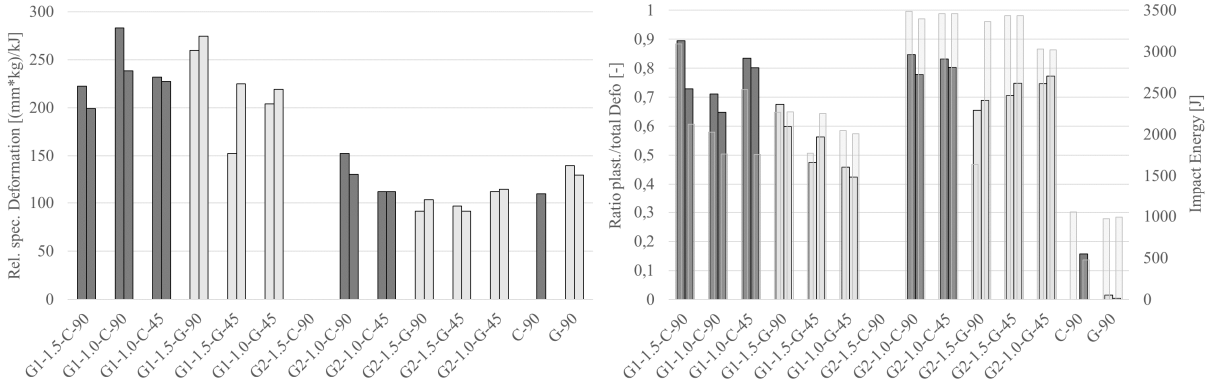

Figure 11. $D_{rel,spec}$ [(mm*kg)/kJ] (left) and the R_{plast} with respect to the impact energy (right).

Regarding the parameter effects on $D_{rel,spec}$, a $[-45/0/45/0]_{2S}$-layup in combination with a *G2*-reinforcement of 1.5 mm and a *GFRP* base structure would yield favourable small value. A *G2*-hybridization of *GFRP* profiles improves the results compared to pure *GFRP*. The share of plastic deformation R_{plast} exhibits a dependency on the impact energy, which emphasizes the nonlinear correlation between the impact energy, the total deformation and its plastic share. Generally *G1*-hybrids and *GFRP*-variants exhibit a lower R_{plast}, respectively. This is particularly observed for pure *FRP* variants and has been mentioned above.

3. Conclusions

The investigation of hybridized *FRP* base structures using steel shells under axial impact loading proved their general applicability in automotive crash structures, because they exhibit a relatively constant load level as well as LU_I- and *SEA* values at least comparable to those of pure *FRPs*.

Excerpt from ISBN 978-3-00-053387-7

Compared to the other variants, the *G1-C-1.0-45* generally exhibited the most advantageous properties. The drop tower bending tests particularly proved a strong hybridization to improve results compared to pure *FRP*. *GFRP*-variants generally outperformed *CFRP*-variants when also considering qualitative aspects such as the severity and areal size of damage. Generally, the direct compatibility and transfer of results based on a large series of hybrid coupon tests previously conducted by the authors remains limited. Considering other aspects, such as compatibility to conventional design and production concepts, scalability or costs [25], hybrids could outperform conventional material systems in those applications. Since there is a highly complex interaction between the two material phases, the effects of - and interdependencies between - the parameters varied in this study are not easily analyzed comprehensively and need further investigations.

Acknowledgments

The authors would like to expess their gratitude to their partners and colleagues at BMW Group and Fraunhofer EMI for valuable discussions and support.

References

[1] European Union. 2009. *Regulation (EC) No 443/2009 of the European Parliament and the Council of 23 April 2009*.
[2] Leohold, J. 2011. *Chancen und Grenzen für eine nachhaltigen FVK-Einsatz im Automobil*. CCeV Automotive Forum 2011, Ingolstadt.
[3] Thornton, P. H. 1979. Energy Absorption in Composite Structures. *Journal of Composite Materials* 13, 3, 247–262.
[4] Friedrich, H., Kopp, J., and Stieg, J. 2003. Composites on the Way to Structural Automotive Applications. *MSF* 426-432, 171–178.
[5] Drechsler, K., Heine, M., Mitschang, P., Baur, W., Gruber, U., Fischer, L., Öttinger, O., Heidenreich, B., Lützenburger, N., and Voggenreiter, H. 2000. Carbon Fiber Reinforced Composites. In *Ullmann's Encyclopedia of Industrial Chemistry*. Wiley-VCH Verlag GmbH & Co. KGaA, Weinheim, Germany.
[6] Koch, B., Knözinger, G., Pleschke, T., and Wolf, H. J. 1999. Hybrid-Frontend als Strukturbauteil. *Kunststoffe* 89, 3, 82–86.
[7] Grasser, S. 2009. *Composite-Metall-Hybridstrukturen unter Berücksichtigung großserientauglicher Fertigungsprozesse*. Symposium Material Innovativ, Ansbach.
[8] Hufenbach, W., Werner, J., and Kiele, J. 2013. Elektromobilität in Ultraleichtbauweise. *ATZ Extra* 18, 2, 42–46.
[9] Feraboli, P., Deleo, F., Wade, B., Rassaian, M., Higgins, M., Byar, A., Reggiani, M., Bonfatti, A., DeOto, L., and Masini, A. 2010. Predictive modeling of an energy-absorbing sandwich structural concept using the building block approach. *Composites Part A: Applied Science and Manufacturing* 41, 6, 774–786.
[10] Frantz, M., Lauter, C., and Tröster, T. 2011. *Advanced manufacturing technologies for automotive structures in multi-material design consisting of high-strength steels and cfrp*, University of Paderborn.
[11] Eckstein, L., Ickert, L., Goede, M., and Dölle, N. 2011. Leichtbau-Bodengruppe mit Verstärkungen aus CFK und GFK. *ATZ (ATZ - Automobiltechnische Zeitschrift)* 113, 4, 256–261.
[12] Wang, X. G., Bloch, J. A., and Cesari, D. 1992. Static and dynamic axial crushing of externally reinforced tubes. *ARCHIVE: Proceedings of the Institution of Mechanical Engineers, Part C: Journal of Mechanical Engineering Science 1989-1996 (vols 203-210)* 206, 53, 355–360.
[13] Bouchet, J., Jacquelin, E., and Hamelin, P. 2002. Dynamic axial crushing of combined composite aluminum tube: the role of both reinforcement and surface treatments. *Composite Structures* 56, 1, 87–96.

Excerpt from ISBN 978-3-00-053387-7

[14] Shin, K. C., Lee, J. J., Kim, K. H., Song, M. C., and Huh, J. S. 2002. Axial crush and bending collapse of an aluminum/GFRP hybrid square tube and its energy absorption capability. *Composite Structures* 57, 1-4, 279–287.
[15] Kim, H. C., Shin, D. K., Lee, J. J., and Kwon, J. B. 2014. Crashworthiness of aluminum/CFRP square hollow section beam under axial impact loading for crash box application. *Composite Structures* 112, 1–10.
[16] Bambach, M. and Elchalakani, M. 2007. Plastic mechanism analysis of steel SHS strengthened with CFRP under large axial deformation. *Thin-Walled Structures* 45, 2, 159–170.
[17] Bambach, M., Elchalakani, M., and Zhao, X. 2009. Composite steel–CFRP SHS tubes under axial impact. *Composite Structures* 87, 3, 282–292.
[18] Bambach, M., Jama, H., and Elchalakani, M. 2009. Axial capacity and design of thin-walled steel SHS strengthened with CFRP. *Thin-Walled Structures* 47, 10, 1112–1121.
[19] Bambach, M., Jama, H., and Elchalakani, M. 2009. Static and dynamic axial crushing of spot-welded thin-walled composite steel–CFRP square tubes. *International Journal of Impact Engineering* 36, 9, 1083–1094.
[20] Bambach, M. 2010. Axial capacity and crushing of thin-walled metal, fibre–epoxy and composite metal–fibre tubes. *Thin-Walled Structures* 48, 6, 440–452.
[21] Bambach, M. 2010. Axial capacity and crushing behavior of metal–fiber square tubes – Steel, stainless steel and aluminum with CFRP. *Composites Part B: Engineering* 41, 7, 550–559.
[22] Bambach, M. R. 2013. Fibre composite strengthening of thin-walled steel vehicle crush tubes for frontal collision energy absorption. *Thin-Walled Structures* 66, 15–22.
[23] Mamalis, A., Manolakos, D., Ioannidis, M., and Papapostolou, D. 2005. On the response of thin-walled CFRP composite tubular components subjected to static and dynamic axial compressive loading: experimental. *Composite Structures* 69, 4, 407–420.
[24] Lukaszewicz, D. H.-J. A. 2013. Automotive Composite Structures for Crashworthiness. In *Advanced Composite Materials for Automotive Applications*, A. Elmarakbi, Ed. John Wiley & Sons Ltd, Chichester, UK, 99–127.
[25] Dlugosch, M., Lukaszewicz, D. H.-J. A., Fritsch J., and Hiermaier, S. 2015. *Gewichtsoptimiertes Design crashrelevanter Fahrzeugstrukturen in Hybridbauweise*. crashMAT 2015, Freiburg [Breisgau].
[26] Salzgitter Flachstahl. 2009. *HCT600XD (HC340XD*)*. Mehrphasenstähle zum Kaltumformen - Dualphasenstähle, Salzgitter.
[27] SGL Group. 2014. *PREDO PR-UD CS 300/600 FT102 38*. Technical Data Sheet, Willich.
[28] SGL Group. 2014. *PREDO PR-UD EST 300/300 FT102 35*. Technical Data Sheet, Willich.
[29] SGL Group. 2014. *Epoxid-Prepreg FT102*. Produkt Information Epoxid-Prepreg FT102, Willich.
[30] Dow Automotive AG. 2003. *Betamate 2096*. Technisches Datenblatt.
[31] Engel, S., Boegle, C., Majamaeki, J., Lukaszewicz, D. H.-J. A., and Moeller, F. 2012. Experimental inverstigation of composite structures during dynamic impact. In *ECCM15 - 15th European Conference on Composite Mateials*.
[32] Feindler, N. 2012. *Charakterisierungs- und Simulationsmethodik zum Versagensverhalten energieabsorbierender Faserverbundstrukturen*. Dissertation, Technische Universität München.

Excerpt from ISBN 978-3-00-053387-7